

Lattice QCD calculation of $K \rightarrow \ell\nu_\ell\ell'^+\ell'^-$ decay width

Xin-Yu Tuo,¹ Xu Feng,^{1,2,3,*} Lu-Chang Jin,^{4,5} and Teng Wang¹

¹*School of Physics and State Key Laboratory of Nuclear Physics
and Technology, Peking University, Beijing 100871, China*

²*Collaborative Innovation Center of Quantum Matter, Beijing 100871, China*

³*Center for High Energy Physics, Peking University, Beijing 100871, China*

⁴*Department of Physics, University of Connecticut, Storrs, CT 06269, USA*

⁵*RIKEN-BNL Research Center, Brookhaven National
Laboratory, Building 510, Upton, NY 11973*

(Dated: March 1, 2025)

Abstract

We develop a methodology for the computation of the $K \rightarrow \ell\nu_\ell\ell'^+\ell'^-$ decay width using lattice QCD and present an exploratory study here. We use a scalar function method to account for the momentum dependence of the decay amplitude and adopt the infinite volume reconstruction (IVR) method to reduce the systematic errors such as the temporal truncation effects and the finite-volume effects. We then perform a four-body phase-space integral to obtain the decay width. The only remaining technical problem is the possible power-law finite-volume effects associated with the process of $K \rightarrow \pi\pi\ell\nu_\ell \rightarrow \ell\nu_\ell\ell'^+\ell'^-$, where the intermediate state involves multiple hadrons. In this work, we use a gauge ensemble of twisted mass fermion with a pion mass $m_\pi = 352$ MeV and a nearly-physical kaon mass. At this kinematics, the $\pi\pi$ in the intermediate state cannot be on shell simultaneously as $2m_\pi > m_K$ and the finite-volume effects associate with $\pi\pi$ state are exponentially suppressed. Using the developed methods mentioned above, we calculate the branching ratios for four channels of $K \rightarrow \ell\nu_\ell\ell'^+\ell'^-$, and obtain the results close to the experimental measurements and ChPT predictions. Our work demonstrates the capability of lattice QCD to improve Standard Model prediction in $K \rightarrow \ell\nu_\ell\ell'^+\ell'^-$ decay width.

* xu.feng@pku.edu.cn

I. INTRODUCTION

Kaon decays, especially some rare kaon decays with ultra small branching ratios, play an important role in current high-precision test of Standard Model, and provide excellent channels to probe physics beyond the Standard Model [1]. The experimental and theoretical studies of kaon decays are believed to be more and more important nowadays because kaon decays have both theoretically clean branching ratios in experimental searches and gradually improved Standard Model predictions [2].

As a typical rare decay, $K \rightarrow \ell\nu_\ell\ell'^+\ell'^-$ involves the second-order electroweak interaction, providing a good place to test Standard Model predictions. In experiments, three types of $K \rightarrow \ell\nu_\ell\ell'^+\ell'^-$ decays have been observed: $K \rightarrow e\nu_e e^+e^-$, $K \rightarrow \mu\nu_\mu e^+e^-$ and $K \rightarrow e\nu_e\mu^+\mu^-$, with small branching ratios in the order of $O(10^{-8})$ [3, 4].

In theoretical study, the determination of $K \rightarrow \ell\nu_\ell\ell'^+\ell'^-$ decay width is highly nontrivial due to the non-perturbative nature of kaon internal structure. Since the phase space of $K \rightarrow \ell\nu_\ell\ell'^+\ell'^-$ allows the virtual photon carry relatively large momentum, e.g. the momentum close to the kaon mass, understanding the momentum dependence of the decay amplitude is essential in theoretical calculation of $K \rightarrow \ell\nu_\ell\ell'^+\ell'^-$ decay width. To be specific, in order to describe the internal structure of kaon, five form factors are involved in $K \rightarrow \ell\nu_\ell\ell'^+\ell'^-$ [5]. The momentum dependence of these form factors is non-negligible. In experiments it produced different results by treating the form factors as constants or considering the relevant momentum dependence through a simple vector-meson-dominance model [3]. Therefore, properly including the momentum dependence of the decay amplitude is important for both theoretical predictions and experimental measurements.

Theoretical study of $K \rightarrow \ell\nu_\ell\ell'^+\ell'^-$ amplitude and form factors has been carried out using chiral perturbation theory (ChPT) [5], where form factors are estimated at the next to leading order (NLO), and predictions close to experimental results are obtained. However, one should note that the form factors F_V and F_A are treated as constants at NLO [5], and the momentum dependence only appears at the NNLO [6, 7]. Thus, the theoretical uncertainties due to momentum dependence have not been estimated thoroughly by the past ChPT studies, which leads to a difficulty to directly compare the results between experiments and ChPT.

As a generic non-perturbative approach, lattice QCD can help to improve the SM pre-

dictions of $K \rightarrow \ell\nu_\ell\ell'^+\ell'^-$ decay width. In past few years, some rare kaon decays have been studied successfully using lattice QCD, such as $K^+ \rightarrow \pi^+\nu\bar{\nu}$ [8–11] and $K \rightarrow \pi\ell^+\ell^-$ [12, 13]. Besides, other processes involving both weak and electromagnetic interactions, e.g. the radiative corrections to the leptonic and semileptonic decays, have also been investigated recently [14–21]. It is interesting to have the lattice QCD study extend its horizon to include the $K \rightarrow \ell\nu_\ell\ell'^+\ell'^-$ decay, where the final state involves four daughter particles.

Here we find that a direct lattice QCD calculation of $K \rightarrow \ell\nu_\ell\ell'^+\ell'^-$ decay width is encountered with the following technical problems.

1. General finite-volume effects: In order to calculate the decay width, one needs to know the arbitrary momentum dependence of the decay amplitude. However, through discrete Fourier transformation the lattice data from a finite-volume box can only access discrete momenta. This problem appears as finite-volume effects in the calculation of decay width.
2. Temporal truncation effects: As it is shown in section III, using the hadronic function in coordinate space, we perform an integral in Euclidean time to obtain the hadronic function with an assigned momentum. In the process of $K \rightarrow K\ell'^+\ell'^- \rightarrow \ell\nu_\ell\ell'^+\ell'^-$, the K in the intermediate state carries nonzero momentum and thus the energy of intermediate state is larger than that of the initial/final state. As a result, the time integral converges when the integral range approaches to infinity. However, in the soft-photon region where the four momentum of the electromagnetic current (E, \vec{P}) is close to zero, the integral converges very slowly. Since the lattice temporal extent T is finite, we find that the temporal truncation effects are not negligible. An extrapolation to infinitely large time extent is required to achieve a precise calculation.
3. Complex calculation procedures: The calculation of $K \rightarrow \ell\nu_\ell\ell'^+\ell'^-$ decay width is of particular complication because it involves five hadronic form factors and four-body phase-space integral. One needs to construct a reliable and convenient approach to calculate the decay amplitude at arbitrary momenta and perform the phase-space integral.
4. Specific power-law finite-volume effects associated with $K \rightarrow \pi\pi\ell\nu_\ell \rightarrow \ell\nu_\ell\ell'^+\ell'^-$: This subprocess is essentially a long-distance process involving multihadron in the interme-

Channels	m_{ee} cuts	Lattice ($m_\pi = 352$ MeV)	ChPT[5]	experiments
$\text{Br}[K \rightarrow e\nu_e e^+ e^-]$	140 MeV	$3.29(35) \times 10^{-8}$	3.39×10^{-8}	$2.91(23) \times 10^{-8}$ [3]
$\text{Br}[K \rightarrow \mu\nu_\mu e^+ e^-]$	140 MeV	$11.08(39) \times 10^{-8}$	8.51×10^{-8}	$7.93(33) \times 10^{-8}$ [3]
$\text{Br}[K \rightarrow e\nu_e \mu^+ \mu^-]$	—	$0.94(8) \times 10^{-8}$	1.12×10^{-8}	$1.72(45) \times 10^{-8}$ [4]
$\text{Br}[K \rightarrow \mu\nu_\mu \mu^+ \mu^-]$	—	$1.52(7) \times 10^{-8}$	1.35×10^{-8}	—

Table I. Comparison of branching ratios of $\text{Br}[K \rightarrow \ell\nu_\ell \ell'^+ \ell'^-]$ among lattice QCD (at unphysical pion mass), ChPT and experiments. In order to compare results with ChPT, we choose the same cuts $m_{ee} > 140$ MeV as that in Ref. [5], where m_{ee} is the invariant mass of the e^+e^- pair. For decays with ee^+e^- , the cuts are applied to both invariant masses. (The kaon mass m_K used in the lattice calculation is slightly different from the physical kaon mass $m_{K,\text{phy}}$. For the lattice results, we rescale the cuts for m_{ee} as $\frac{m_{ee}}{m_K} > \frac{140 \text{ MeV}}{m_{K,\text{phy}}}$.) The experimental results of $K \rightarrow e\nu_e e^+ e^-$ and $K \rightarrow \mu\nu_\mu e^+ e^-$ are the extrapolated values from $m_{ee} > 150$ MeV and 145 MeV to $m_{ee} > 140$ MeV. The extrapolation formula are given in Ref. [3].

diate state. When the momentum of the electromagnetic current is fixed, the corresponding power-law finite-volume effects have been studied first by Ref. [22] using the K_L - K_S mass difference as an example and later by Ref. [23] for more general cases. When calculating the decay width, the momentum of the electromagnetic current runs over the whole allowed phase-space region, the finite-volume correction becomes more complicated and still remains an open problem. Thus situation also happens for the $K \rightarrow \mu^+ \mu^-$ decay where two off-shell photons are involved [24].

This work is aiming at solving the first three technical problems, building a convenient calculation procedure and presenting the lattice results of $K \rightarrow \ell\nu_\ell \ell'^+ \ell'^-$ decay width. The central part of this paper is to introduce the following methodologies: 1) a scalar function method to compute the hadronic function, 2) infinite volume reconstruction (IVR) method[25] to reduce the unphysical temporal truncation and finite-volume effects, and 3) convenient phase-space integration method to obtain the decay width.

With these developed methods, we calculate $K \rightarrow \ell\nu_\ell \ell'^+ \ell'^-$ decay width using a gauge ensemble of $N_f = 2 + 1 + 1$ -flavor twisted mass fermion at the unphysical pion mass $m_\pi = 0.3515(15)$ GeV. The valance strange quark mass is tuned to make the kaon mass

$m_K = 0.5057(13)$ GeV close to its physical value. The lattice results of the branching ratios are summarized in Table I and are found to be close to experimental measurements and ChPT predictions. Residual systematic errors of our lattice calculation mainly come from unphysical quark mass and non-zero lattice spacing. Calculation at the physical quark mass together with the continuum extrapolation will be included in our future work.

In this paper we will first introduce in Sec. II the decay amplitude of $K \rightarrow \ell\nu_\ell\ell'^+\ell'^-$ in Minkowski space. This part follows Refs. [5, 26] and is also a necessary part of lattice calculation. In Sec. III we will establish a connection between Minkowski hadronic function and Euclidean one, and give more detailed description of the computational techniques mentioned above, which is the most central part of this paper. Finally, we present the numerical results in Sec. IV and reach a conclusion in Sec. V.

II. DECAY WIDTH OF $K \rightarrow \ell\nu_\ell\ell'^+\ell'^-$

Our program aims at the calculation of the branching ratios of $K \rightarrow \ell\nu_\ell\ell'^+\ell'^-$ via

$$\text{Br} [K \rightarrow \ell\nu_\ell\ell'^+\ell'^-] = \frac{1}{2m_K\Gamma_K} \int d\Phi_4 |\mathcal{M}(K \rightarrow \ell\nu_\ell\ell'^+\ell'^-)|^2, \quad (1)$$

where $\Gamma_K = 5.3168(86) \times 10^{-14}$ MeV is the kaon decay width from the Particle Data Group [27].¹ $\mathcal{M}(K \rightarrow \ell\nu_\ell\ell'^+\ell'^-)$ is the decay amplitude and $\int d\Phi_4$ indicates a four-body phase-space integral.

Our approach to calculate the $K \rightarrow \ell\nu_\ell\ell'^+\ell'^-$ decay width includes three major steps. The first step is to determine the Minkowski hadronic functions

$$\begin{aligned} H_M^\nu(q) &= \langle 0 | J_{W,M}^\nu(0) | K(q) \rangle, \\ H_M^{\mu\nu}(p, q) &= \int d^4x e^{ip \cdot x} \langle 0 | T \{ J_{\text{em},M}^\mu(x) J_{W,M}^\nu(0) \} | K(q) \rangle, \end{aligned} \quad (2)$$

where the electromagnetic and weak currents in Minkowski space are defined as $J_{\text{em},M}^\mu = \frac{2}{3}\bar{u}\gamma^\mu u - \frac{1}{3}\bar{d}\gamma^\mu d - \frac{1}{3}\bar{s}\gamma^\mu s$ and $J_{W,M}^\nu = \bar{s}\gamma^\nu(1 - \gamma_5)u$. $p = (E, \vec{p})$ and $q = (m_K, \vec{0})$ are Minkowski 4-momentum of the electromagnetic current and initial kaon state. We define the parameters ρ_1 and ρ_2 as

$$p^2 = \rho_1 m_K^2, \quad (q - p)^2 = \rho_2 m_K^2. \quad (3)$$

¹ Note that we do not calculate the total kaon decay width from lattice.

In a lattice QCD study, the hadronic functions are generally calculated in Euclidean space. The connection between Minkowski and Euclidean hadronic function is established in Sec. III.

As a second step, the decay amplitude $\mathcal{M}(K \rightarrow \ell \nu_\ell \ell'^+ \ell'^-)$ is constructed by combining the hadronic function $H_M^{\mu\nu}(p, q)$ with the leptonic factor [5]. Here we target on the determination of the amplitude \mathcal{M} with arbitrary momentum dependence.

As a last step, the decay amplitude is used as an input in the integral (1) to obtain the decay width. The definition of four-body phase-space integral is provided in Ref. [26], which is originally used for the process of $K \rightarrow \ell \bar{\ell} \ell' \bar{\ell}'$. We use the Monte Carlo method to perform the phase-space integration.

A. Hadronic function in Minkowski space

In the continuum theory the hadronic function $H_M^{\mu\nu}(p, q)$ satisfies Ward identity [5]

$$p_\mu H_M^{\mu\nu}(p, q) = f_K q^\nu \quad (4)$$

with f_K the kaon decay constant. Using Ward identity, $H_M^{\mu\nu}(p, q)$ can be written in terms of five form factors [19] as

$$\begin{aligned} H_M^{\mu\nu}(p, q) = & H_1 [p^2 g^{\mu\nu} - p^\mu p^\nu] + H_2 [(p \cdot q - p^2) p^\mu - p^2 (q - p)^\mu] (q - p)^\nu \\ & - i \frac{F_V}{m_K} \varepsilon^{\mu\nu\alpha\beta} p_\alpha q_\beta + \frac{F_A}{m_K} [(q \cdot p - p^2) g^{\mu\nu} - (q - p)^\mu p^\nu] \\ & + f_K \left[g^{\mu\nu} + \frac{(2q - p)^\mu (q - p)^\nu}{2q \cdot p - p^2} \right]. \end{aligned} \quad (5)$$

Using the hadronic function $H_M^\nu(q)$, one can construct the amplitude for the subprocess of $K \rightarrow \ell \nu_\ell \rightarrow \ell \nu_\ell \ell'^+ \ell'^-$ as shown in Fig. 1. Using the hadronic function $H_M^{\mu\nu}(p, q)$, the remaining contribution to the decay amplitude of $K \rightarrow \ell \nu_\ell \ell'^+ \ell'^-$ can be constructed. For the case of $\ell' = \ell$ the decay amplitude consists of two parts, shown as the ‘‘Direct’’ and ‘‘Exchange’’ diagrams in Fig. 2. For $\ell \neq \ell'$, only ‘‘Direct’’ diagram contributes.

Here we use the case of $\ell' = \ell$ to introduce the expressions for the decay amplitudes. The 4-momenta of the final-state leptons are defined as p_i with $i = 1, 2, 3, 4$ as shown in Fig. 2.

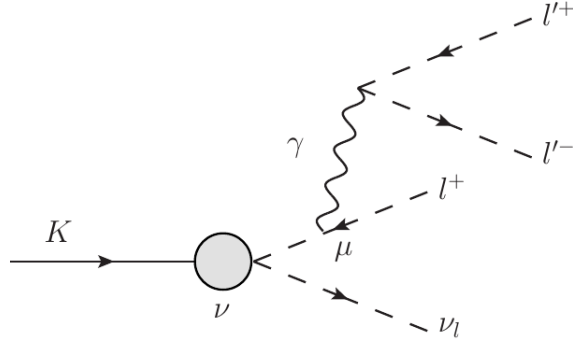


Figure 1. Contribution of off-shell photon radiation from the final-state lepton in $K \rightarrow \ell\nu_\ell\ell'^+\ell'^-$. The hadronic part is described by $H_M^\nu(q)$.

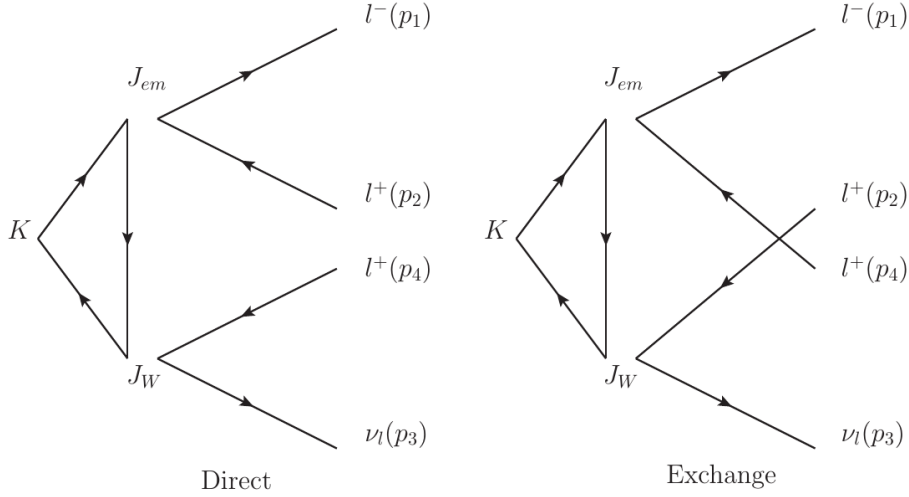


Figure 2. Contribution of off-shell photon radiation from quarks in $K \rightarrow \ell\nu_\ell\ell^+\ell^-$. The hadronic part is described by $H_M^{\mu\nu}(p, q)$.

The decay amplitudes are given as

$$\begin{aligned}
 i\mathcal{M}_D &= -i \frac{G_F e^2 V_{us}^*}{\sqrt{2} s_{12}} [f_K L^\mu(p_1, p_2, p_3, p_4) - H_M^{\mu\nu}(p_{12}, q) l_\nu(p_3, p_4)] [\bar{u}(p_1) \gamma_\mu v(p_2)], \\
 i\mathcal{M}_E &= +i \frac{G_F e^2 V_{us}^*}{\sqrt{2} s_{14}} [f_K L^\mu(p_1, p_4, p_3, p_2) - H_M^{\mu\nu}(p_{14}, q) l_\nu(p_3, p_2)] [\bar{u}(p_1) \gamma_\mu v(p_4)], \quad (6)
 \end{aligned}$$

where the terms with a factor of f_K arise from Fig. 1, which has both the ‘‘Direct’’ and the ‘‘Exchange’’ contribution if $l = l'$, and the terms with a factor of $H_M^{\mu\nu}$ come from Fig. 2. Here \mathcal{M}_D and \mathcal{M}_E stand for the amplitudes from the ‘‘Direct’’ and ‘‘Exchange’’ diagrams, respectively. The photon momentum is given by $p_{ij} \equiv p_i + p_j$ and $s_{ij} \equiv p_{ij}^2$ is the momentum

square. The leptonic factors L^μ and l^μ are defined as

$$\begin{aligned} l^\mu(p_3, p_4) &= \bar{u}(p_3) \gamma^\mu (1 - \gamma_5) v(p_4), \\ L^\mu(p_1, p_2, p_3, p_4) &= l^\mu(p_3, p_4) + L'^\mu(p_1, p_2, p_3, p_4), \end{aligned} \quad (7)$$

with

$$L'^\mu(p_1, p_2, p_3, p_4) = m_\ell \bar{u}(p_3) (1 + \gamma_5) \frac{2p_4^\mu + \not{p}_{12} \gamma^\mu}{m_\ell^2 - (p_4 + p_{12})^2} v(p_4). \quad (8)$$

Note that \bar{u} and v in Eqs. (7) and (8) stand for the spinors of ℓ and ν_ℓ , which form a charged weak current, while \bar{u} and v in Eq. (6) stand for the spinors of ℓ^+ and ℓ^- from an electromagnetic current. Finally, V_{us}^* is the CKM matrix element and G_F is the Fermi constant.

It should be noticed that, the term $f_K g^{\mu\nu}$ in Eq. (5) can produce a contribution proportional to $f_K l^\mu$, which exactly cancels the $f_K l^\mu$ term contained by $f_K L^\mu$ in Eq. (6). We find that the $f_K l^\mu$ term from Fig. 1 would be IR divergent in the limit of vanishing lepton mass. In order to maintain the exact cancellation in the large IR contribution and reduce the statistical uncertainty, we replace $H_M^{\mu\nu}$ by $H'_M{}^{\mu\nu}$ in Eq. 6, with $H'_M{}^{\mu\nu}$ defined as

$$H'_M{}^{\mu\nu}(p, q) \equiv H_M^{\mu\nu}(p, q) - f_K g^{\mu\nu} = H_M^{\mu\nu}(p, q) - \frac{p_\rho H_M^{\rho 0}(p, q)}{m_K} g^{\mu\nu}. \quad (9)$$

In this way, the amplitude \mathcal{M}_D and \mathcal{M}_E can be written as

$$\begin{aligned} i\mathcal{M}_D &= -i \frac{G_F e^2 V_{us}^*}{\sqrt{2} s_{12}} [f_K L'^\mu(p_1, p_2, p_3, p_4) - H'_M{}^{\mu\nu}(p_{12}, q) l_\nu(p_3, p_4)] [\bar{u}(p_1) \gamma_\mu v(p_2)], \\ i\mathcal{M}_E &= +i \frac{G_F e^2 V_{us}^*}{\sqrt{2} s_{14}} [f_K L'^\mu(p_1, p_4, p_3, p_2) - H'_M{}^{\mu\nu}(p_{14}, q) l_\nu(p_3, p_2)] [\bar{u}(p_1) \gamma_\mu v(p_4)]. \end{aligned} \quad (10)$$

Using \mathcal{M}_D and \mathcal{M}_E as input, the branching ratio of $K \rightarrow \ell \nu_\ell \ell'^+ \ell'^-$ for $\ell = \ell'$ can be calculated through

$$\text{Br}[K \rightarrow \ell \nu_\ell \ell'^+ \ell'^-] = \frac{1}{2m_K \Gamma_K} \int d\Phi_4 (|\mathcal{M}_D|^2 + |\mathcal{M}_E|^2 + 2 \text{Re}[\mathcal{M}_D \mathcal{M}_E^*]). \quad (11)$$

For $\ell \neq \ell'$, we only have the $|\mathcal{M}_D|^2$ term in the above equation:

$$\text{Br}[K \rightarrow \ell \nu_\ell \ell'^+ \ell'^-] = \frac{1}{2m_K \Gamma_K} \int d\Phi_4 |\mathcal{M}_D|^2. \quad (12)$$

B. Phase-space integral

The definition of four-body phase-space integral follows Ref. [26]. In Ref. [26] the formulae are simplified for the case of the daughter particles with the same masses. Here we generalize the formulae to the case that the daughter particles have different masses.

The four-body phase-space $d\Phi_4$ is defined as:

$$d\Phi_4 = \frac{\mathcal{S}\lambda m_K^4}{2^{14}\pi^6} dx_{12} dx_{34} dy_{12} dy_{34} d\phi. \quad (13)$$

Here \mathcal{S} is a symmetry factor with $\mathcal{S} = 1$ for the case of $\ell \neq \ell'$ and $\mathcal{S} = \frac{1}{2}$ for $\ell = \ell'$. The phase-space variables x_{12} , x_{34} , y_{12} , y_{34} and ϕ are five independent Lorentz invariant quantities with x_{ij} and y_{ij} defined as

$$x_{12} = \frac{s_{12}}{m_K^2}, \quad x_{34} = \frac{s_{34}}{m_K^2}, \quad y_{12} = \frac{2\bar{p}_{12} \cdot p_{34} - 2p_{12} \cdot p_{34}\delta_{12}}{\lambda m_K^2}, \quad y_{34} = \frac{2\bar{p}_{34} \cdot p_{12} - 2p_{12} \cdot p_{34}\delta_{34}}{\lambda m_K^2}, \quad (14)$$

where $\bar{p}_{ij} \equiv p_i - p_j$, $\lambda \equiv \sqrt{(1 - x_{12} - x_{34})^2 - 4x_{12}x_{34}}$ and $\delta_{ij} \equiv \frac{m_i^2 - m_j^2}{s_{ij}}$. The indices 1, 2, 3, 4 specify the particles in the final state. The quantity ϕ can be expressed as

$$\epsilon_{\mu\nu\rho\sigma} p_1^\mu p_2^\nu p_3^\rho p_4^\sigma = -\frac{\lambda m_K^4 \omega}{16} \sqrt{(\lambda_{12}^2 - y_{12}^2)(\lambda_{34}^2 - y_{34}^2)} \sin \phi \quad (15)$$

with

$$\lambda_{ij} = \sqrt{\left(1 - \frac{m_i^2}{s_{ij}} - \frac{m_j^2}{s_{ij}}\right)^2 - 4\frac{m_i^2 m_j^2}{s_{ij}^2}}, \quad \omega = 2\sqrt{x_{12}x_{34}}. \quad (16)$$

To create a Monte Carlo generator, it is useful to assign each particle a 4-momentum in the rest frame of kaon in terms of the phase-space variables as

$$\begin{aligned} E_{1(2)} &= m_K \frac{(1 + \delta)(1 \pm \delta_{12}) \pm \lambda y_{12}}{4}, & E_{3(4)} &= m_K \frac{(1 - \delta)(1 \pm \delta_{34}) \pm \lambda y_{34}}{4}, \\ \vec{p}_{1(2)} &= \mp m_K \sqrt{\frac{x_{12}}{4}(\lambda_{12}^2 - y_{12}^2)} \hat{x} + m_K \frac{\lambda(1 \pm \delta_{12}) \pm (1 + \delta)y_{12}}{4} \hat{y}, \\ \vec{p}_{3(4)} &= m_K \sqrt{\frac{x_{34}}{4}(\lambda_{34}^2 - y_{34}^2)} (\mp \cos \phi \hat{x} \pm \sin \phi \hat{z}) - m_K \frac{\lambda(1 \pm \delta_{34}) \pm (1 - \delta)y_{34}}{4} \hat{y}, \end{aligned} \quad (17)$$

with $\delta \equiv x_{12} - x_{34}$. The range of the phase-space variables are adjusted as

$$\begin{aligned} \left(\frac{m_1 + m_2}{m_K}\right)^2 &\leq x_{12} \leq \left(1 - \frac{m_3 + m_4}{m_K}\right)^2, \\ \left(\frac{m_3 + m_4}{m_K}\right)^2 &\leq x_{34} \leq (1 - \sqrt{x_{12}})^2, \\ -\lambda_{ij} &\leq y_{ij} \leq \lambda_{ij}, \quad 0 \leq \phi \leq 2\pi. \end{aligned} \quad (18)$$

III. METHODOLOGIES OF LATTICE CALCULATION

The $K \rightarrow \ell \nu_\ell \ell'^+ \ell'^-$ decay involves five form factors as given in Eq. 5. The classification of these form factors requires the constraint from Ward identity. In the lattice calculation, Ward identity can be easily violated either by the lattice artifacts, e.g. due to the usage of local vector current, or by the finite-volume effects, e.g. due to the usage of the arbitrary momentum. These systematic effects significantly affect the precise determination of the form factors from lattice QCD. Note that our target is to calculate the total decay width and the determination of each individual form factor is not a necessary step. In this work we develop an approach called *scalar function method*, which provides a convenient way to represent the lattice results for coordinate space matrix elements. Momentum space matrix elements can be obtained from the scalar function representation with automatic rotational averaging. The IVR method is then applied to make the corrections of the temporal truncation effects and finite-volume effects for the decay amplitude. More details of the methodologies are given as follows.

A. Construction of Minkowski hadronic function using lattice data

In order to reproduce Minkowski hadronic function using Euclidean lattice data, we shall first establish the relation between the hadronic functions in Euclidean and Minkowski spacetime.

In Euclidean spacetime, the hadronic function is defined as:

$$H_E^{\mu\nu}(x, Q) = \langle 0 | T \{ J_{\text{em}}^\mu(x) J_W^\nu(0) \} | K(Q) \rangle, \quad (19)$$

where $Q = (im_K, \vec{0})$ is the Euclidean 4-momentum of initial kaon state. $H_E^{\mu\nu}(x, Q)$ can be extracted from a three-point correlation function $C^{\mu\nu}(\vec{x}, t; \Delta T)$

$$C^{\mu\nu}(\vec{x}, t; \Delta T) = \begin{cases} \left\langle J_{\text{em}}^\mu(\vec{x}, t) J_W^\nu(\vec{0}, 0) \phi_K^\dagger(-\Delta T) \right\rangle, & t \geq 0, \\ \left\langle J_W^\mu(\vec{0}, 0) J_{\text{em}}^\nu(\vec{x}, t) \phi_K^\dagger(t - \Delta T) \right\rangle, & t < 0. \end{cases} \quad (20)$$

We choose sufficiently large ΔT to guarantee kaon ground-state dominance. Then the hadronic function $H_E^{\mu\nu}(\vec{x}, t)$ can be determined through

$$H_{E,A/V}^{(L),\mu\nu}(\vec{x}, t) = \begin{cases} N_K^{-1} Z_V Z_{A/V} e^{m_K \Delta T} C_{A/V}^{\mu\nu}(\vec{x}, t, \Delta T), & t \geq 0, \\ N_K^{-1} Z_V Z_{A/V} e^{m_K(\Delta T - t)} C_{A/V}^{\mu\nu}(\vec{x}, t, \Delta T), & t < 0. \end{cases} \quad (21)$$

In Eq. (21) we have separated the weak current into axial-vector-current and vector-current parts by using the subscript A/V . Z_A and Z_V are the corresponding renormalization factors. We use the superscript (L) to emphasize that this hadronic function is calculated in the finite volume. The normalization factor $N_K = \langle K | \phi_K^\dagger(0) | 0 \rangle / (2m_K)$ and the kaon mass m_K can be calculated from the lattice two-point functions.

For simplicity, let us first consider the infinite-volume Euclidean hadronic function $H_E^{\mu\nu}(x, Q)$. In momentum space it is given by

$$H_E^{\mu\nu}(P, Q) = -i \int_{-T/2}^{T/2} dt \int d^3\vec{x} e^{Et - i\vec{p}\cdot\vec{x}} H_E^{\mu\nu}(x, Q) \quad (22)$$

with the Euclidean momenta

$$P = (iE, \vec{p}), \quad -P^2 = \rho_1 m_K^2, \quad -(Q - P)^2 = \rho_2 m_K^2. \quad (23)$$

In order to calculate decay width, the Euclidean function $H_E^{\mu\nu}(P, Q)$ should be related to Minkowski one $H_M^{\mu\nu}(p, q)$, which is defined in Sec. II. This relation can be established by inserting the complete set of intermediate states into $H_M^{\mu\nu}(p, q)$ through

$$\begin{aligned} H_M^{\mu\nu}(p, q) &= \int_0^\infty dt \sum_n \langle 0 | J_{\text{em}, M}^\mu(0) | n(\vec{p}) \rangle_M \langle n(\vec{p}) | J_{W, M}^\nu(0) | K(q) \rangle_M e^{i(E - E_n + i\epsilon)t} \\ &+ \int_{-\infty}^0 dt \sum_{n_s} \langle 0 | J_{W, M}^\nu(0) | n_s(-\vec{p}) \rangle_M \langle n_s(-\vec{p}) | J_{\text{em}, M}^\mu(0) | K(q) \rangle_M e^{i(E + E_{n_s} - m_K - i\epsilon)t} \\ &= i \sum_n \frac{1}{E - E_n + i\epsilon} \langle 0 | J_{\text{em}, M}^\mu(0) | n(\vec{p}) \rangle_M \langle n(\vec{p}) | J_{W, M}^\nu(0) | K(q) \rangle_M \\ &- i \sum_{n_s} \frac{1}{E + E_{n_s} - m_K - i\epsilon} \langle 0 | J_{W, M}^\nu(0) | n_s(-\vec{p}) \rangle_M \langle n_s(-\vec{p}) | J_{\text{em}, M}^\mu(0) | K(q) \rangle_M. \quad (24) \end{aligned}$$

For $t > 0$ and $t < 0$, the intermediate states are denoted as the state $|n\rangle$ with strangeness $S = 0$ and the state $|n_s\rangle$ with $S = 1$, respectively. The matrix elements $\langle \dots \rangle_M$ carry a subscript M , which reminds us that it is defined in Minkowski space. The low-lying states for $|n\rangle$ are given by the p -wave $\pi\pi$ states, which couple to the ρ resonance. The lowest state for $|n_s\rangle$ is given by $|K\rangle$ state. The relevant diagrams for these low-lying states are shown in Figs. 3 and 4.

When inserting the complete set of intermediate states into the Euclidean function

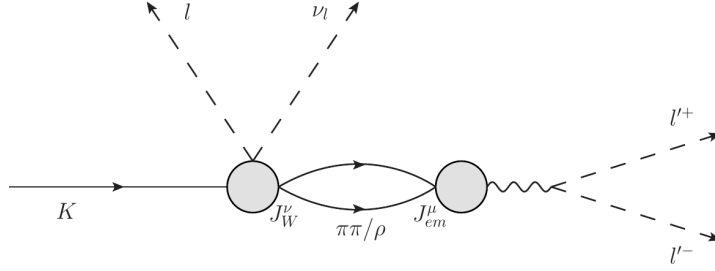


Figure 3. Low-lying-state dominance for $t > 0$: $\pi\pi$ or ρ states.

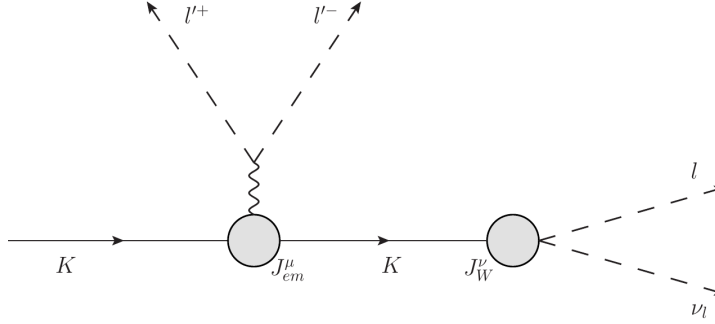


Figure 4. Low-lying-state dominance for $t < 0$: kaon states.

$H_E^{\mu\nu}(P, Q)$, we have

$$\begin{aligned}
H_E^{\mu\nu}(P, Q) &= -i \int_0^{T/2} dt \sum_n \langle 0 | J_{em}^\mu(0) | n \rangle_E \langle n | J_W^\nu(0) | K(Q) \rangle_E e^{(E-E_n)t} \\
&\quad -i \int_{-T/2}^0 dt \sum_{n_s} \langle 0 | J_W^\nu(0) | n_s \rangle_E \langle n_s | J_{em}^\mu(0) | K(Q) \rangle_E e^{(E+E_{n_s}-m_K)t} \\
&= i \sum_n \frac{1 - e^{-(E_n-E)T/2}}{E - E_n} \langle 0 | J_{em}^\mu(0) | n \rangle_E \langle n | J_W^\nu(0) | K(Q) \rangle_E \\
&\quad -i \sum_{n_s} \frac{1 - e^{-(E+E_{n_s}-m_K)T/2}}{E + E_{n_s} - m_K} \langle 0 | J_W^\nu(0) | n_s \rangle_E \langle n_s | J_{em}^\mu(0) | K(Q) \rangle_E. \quad (25)
\end{aligned}$$

Different from the Minkowski expression, we have introduced a time integral range $[-T/2, T/2]$ to define the Euclidean hadronic function. This is because the state n consists of a continuous set of $\pi\pi$ state. When $E_n = E_{\pi\pi} < E$, the factor $e^{-(E_n-E)T/2}$ exponentially grows as T increases. In this case, one needs to use the finite-volume hadronic function $H_E^{(L),\mu\nu}(P, Q)$, where the low-lying $\pi\pi$ states are discrete. When a spatial momentum \vec{p} is assigned, one can remove the exponential factor of $e^{-(E_n-E)T/2}$ by isolating each low-lying $\pi\pi$ state. After that, the difference between $H_E^{(L),\mu\nu}(P, Q)$ and the real part of $H_M^{\mu\nu}(p, q)$ can be taken into account by the finite-volume correction formula developed in Refs. [22, 23]. The imaginary

part of $H_M^{\mu\nu}(p, q)$ can be reproduced by calculating the on-shell decay amplitudes $K \rightarrow \pi\pi\ell\nu$ and $\gamma^* \rightarrow \pi\pi$, where the finite-volume technique is mature [28, 29]. The timelike pion form factor from $\gamma^* \rightarrow \pi\pi$ has been calculated on lattice since 2014 [30–32].

In this study, we perform the calculation at the unphysical pion mass $m_\pi = 0.3515(15)$ GeV. As a result, $E_{\pi\pi} - E$ is always larger than zero. In this case one could take the limit of $T \rightarrow \infty$ and use the relation between Euclidean and Minkowski matrix element (due to the different convention for the J^μ operator):

$$\langle A|J^\mu(0)|B\rangle_E = \begin{cases} \langle A|J^\mu(0)|B\rangle_M, & \mu = 0 \\ -i\langle A|J^\mu(0)|B\rangle_M, & \mu = 1, 2, 3 \end{cases} \quad (26)$$

with J^μ either electromagnetic or weak current. It is easy to verify that

$$H_E^{\mu\nu}(P, Q)|_{T \rightarrow \infty} = c^{\mu\nu} H_M^{\mu\nu}(p, q) \quad (27)$$

with $c^{00} = 1$, $c^{0i} = c^{i0} = -i$ and $c^{ij} = -1$. Thus we have shown that the Minkowski hadronic function can be calculated by Euclidean lattice data.

B. Scalar function method

In the following part of the paper, for simplicity we will omit the subscript E in the Euclidean hadronic function and use $H^{\mu\nu}(x, Q)$ and $H^{\mu\nu}(P, Q)$ to replace $H_E^{\mu\nu}(P, Q)$, $H_E^{\mu\nu}(x, Q)$. It is straightforward to compute $H^{\mu\nu}(P, Q)$ using the 4×4 Lorentz tensor $H^{\mu\nu}(x, Q)$ as input

$$H^{\mu\nu}(P, Q) = -i \int_{-T/2}^{T/2} dt \int d^3\vec{x} e^{Et - i\vec{p}\cdot\vec{x}} H^{\mu\nu}(x, Q). \quad (28)$$

We call this method as the *direct method*.

In a realistic lattice calculation, $H^{\mu\nu}(x, Q)$ is given by the finite-volume lattice data $H^{(L),\mu\nu}(x, Q)$. The data depends on $L^3 \times T$ spacetime coordinates, 4×4 Lorentz indices and two types of current insertions (V/A). Take a $24^3 \times 48$ lattice as an example, the data size is about 650 MB per configuration as shown in Table II. The computation of the decay width requires the integration using $H^{(L),\mu\nu}(x, Q)$ as input and is thus quite complicated.

In this work we propose a new method, called as *scalar function method*, which could significantly reduce the size of data input and provide automatic rotational averaging. The simplification can be achieved by converting $H^{\mu\nu}(P, Q)$ and $H^{\mu\nu}(x, Q)$ into the Lorentz scalar

Method	Direct method	Scalar function method
Stored data	$H^{(L),\mu\nu}(x, Q)$	$I_i^{(L)}(\vec{x} ^2, t)$
Space-time dimentions	$(L, L, L, T) : 24^3 \times 48$	$(r_{\max}^2, T) : 432 \times 48$
Other dimentions	$(\mu, \nu, V/A) : 4 \times 4 \times 2$	6
Data size	≈ 650 MB/conf	≈ 2 MB/conf

Table II. Comparison of the size of input data required by scalar function method and direct method. By using scalar function method, the hadronic function $H^{\mu\nu}(x, Q)$ is converted into six scalar functions $I_i(|\vec{x}|^2, t)$. The former requires the total data size of $L^3 \times T \times 4 \times 4 \times 2$ while the latter only requires $r_{\max}^2 \times T \times 6$ with $r_{\max}^2 \equiv 3(L/2)^2$. As the lattice size L increases, the scalar function method become more efficient compared the direct one.

functions. For example, $H^{\mu\nu}(P, Q)$ can be used to construct the following Lorentz invariant quantities

$$\begin{aligned}
\tilde{I}_1(\rho_1, \rho_2) &= -\delta^{\mu\nu} m_K^2 H^{\mu\nu}(P, Q), & \tilde{I}_2(\rho_1, \rho_2) &= Q^\mu Q^\nu H^{\mu\nu}(P, Q), \\
\tilde{I}_3(\rho_1, \rho_2) &= P^\mu Q^\nu H^{\mu\nu}(P, Q), & \tilde{I}_4(\rho_1, \rho_2) &= Q^\mu P^\nu H^{\mu\nu}(P, Q), \\
\tilde{I}_5(\rho_1, \rho_2) &= P^\mu P^\nu H^{\mu\nu}(P, Q), & \tilde{I}_6(\rho_1, \rho_2) &= \epsilon^{\mu\nu\alpha\beta} P^\alpha Q^\beta H^{\mu\nu}(P, Q).
\end{aligned} \tag{29}$$

Since the momentum Q satisfies the on-shell condition $Q^2 = -m_K^2$, the quantities $\tilde{I}_i(\rho_1, \rho_2)$ only depend on two variables ρ_1 and ρ_2 , which are defined in Eq. (23). Then we can write $H^{\mu\nu}(P, Q)$ as a combination of

$$H^{\mu\nu}(P, Q) = \sum_{i=1}^6 \tilde{w}_i^{\mu\nu}(P, Q) \tilde{I}_i(\rho_1, \rho_2), \tag{30}$$

where $\tilde{w}_i^{\mu\nu}(P, Q)$ are analytically known Lorentz factors. The way to obtain $\tilde{w}_i^{\mu\nu}(P, Q)$ has been discussed in Appendix A.

For $H^{\mu\nu}(x, Q)$, we can also write them in terms of Lorentz invariant quantities through

$$H^{\mu\nu}(x, Q) = \sum_{i=1}^6 w_i^{\mu\nu}(x, Q) I_i(|\vec{x}|^2, t), \tag{31}$$

where I_i are defined as

$$\begin{aligned}
I_1(|\vec{x}|^2, t) &= \delta^{\mu\nu} H^{\mu\nu}(x, Q), \\
I_2(|\vec{x}|^2, t) &= -\frac{Q^\mu Q^\nu}{m_K^2} H^{\mu\nu}(x, Q) = H^{00}(x, Q), \\
I_3(|\vec{x}|^2, t) &= \frac{x^\mu Q^\nu}{im_K} H^{\mu\nu}(x, Q) - \frac{x \cdot Q}{im_K} I_2 = x^i H^{i0}(x, Q), \\
I_4(|\vec{x}|^2, t) &= x^i H^{0i}(x, Q), \\
I_5(|\vec{x}|^2, t) &= x^\mu x^\nu H^{\mu\nu}(x, Q) - \frac{x \cdot Q}{im_K} (I_3 + I_4) - \left(\frac{x \cdot Q}{im_K}\right)^2 I_2 = x^i x^j H^{ij}(x, Q), \\
I_6(|\vec{x}|^2, t) &= \epsilon^{\mu\nu\alpha 0} x^\alpha H^{\mu\nu}(x, Q).
\end{aligned} \tag{32}$$

It is more convenient to write I_i as the functions of the variables $(|\vec{x}|^2, t) = (x^2 - (x \cdot Q)^2 / (im_K)^2, (x \cdot Q) / (im_K))$. Again, $w_i^{\mu\nu}(x, Q)$ are also the known factors. The choice of the scalar functions is not unique. Here we design the scalar functions using the simple combination of x^μ and $H^{\mu\nu}(x, Q)$.

We then put Eqs. (29) and (32) into Eq. (28) and obtain a relation between $I_j(|\vec{x}|^2, t)$ and $\tilde{I}_i(\rho_1, \rho_2)$

$$\tilde{I}_i(\rho_1, \rho_2) = \int d^4x \phi_{ij}(\rho_1, \rho_2; |\vec{x}|^2, t) I_j(|\vec{x}|^2, t). \tag{33}$$

The detailed expressions for $\phi_{ij}(\rho_1, \rho_2; |\vec{x}|^2, t)$ are given in Appendix A. Note that in $I_j(|\vec{x}|^2, t)$ the index j belongs to $1 \leq j \leq 6$, $|\vec{x}|^2$ takes values from $[0, r_{\max}^2 \equiv 3(L/2)^2]$ and t ranges from $[-T/2, T/2]$. Thus the total data size for $I_j(|\vec{x}|^2, t)$ is accounted as $\sim 6 \times r_{\max}^2 \times T$, which is significantly smaller than the size of $H^{\mu\nu}(x, Q)$. A comparison is made in Table II to demonstrate the efficiency of the scalar function method.

Using $I_j(|\vec{x}|^2, t)$ as input and adopting Eqs. (33), and (30), the hadronic function $H^{\mu\nu}(P, Q)$ can be constructed for arbitrary momenta P . Then the decay amplitude $\mathcal{M}(K \rightarrow \ell\nu\ell'^+\ell'^-)$ can be determined.

C. IVR method

When utilizing Eq. (28), it shall be pointed out that $H^{\mu\nu}(x, Q)$ needs to be replaced by the finite-volume lattice data $H^{(L),\mu\nu}(x, Q)$. As the lattice simulation is performed with a finite temporal extend T and spatial extent L , the replacement will cause the temporal truncation effects and finite-volume effects.

In this section, we will use the IVR method [25] to perform the correction for both temporal truncation and finite-volume effects. The idea of the IVR method is that “infinite-volume data” $H^{\mu\nu}(x, Q)$ can be reconstructed from the finite-volume lattice data $H^{(L),\mu\nu}(x, Q)$. This method has been successfully applied to various calculation such as neutrinoless double beta decay [33], pion charge radius [34], electromagnetic correction to leptonic decay [18] and rare kaon decay [35]. In this work, the IVR method is separated into two steps, namely IVR and δ_{IVR} . The former mainly corrects the temporal truncation effects, and the latter focuses on the finite-volume effects.

For simplicity, we will discuss IVR techniques using $H^{\mu\nu}(x, Q)$ and $H^{\mu\nu}(P, Q)$, and leave IVR formulae for the scalar functions $I_i(|\vec{x}|^2, t)$ and $\tilde{I}_i(\rho_1, \rho_2)$ in Appendix A. It should be reminded that the formulae in Appendix A is what we have actually used in the numerical calculation.

1. Temporal truncation effects

We start the discussion from the temporal truncation effects. As shown in Eq. (25), when the temporal extent T increases, the unphysical terms either exponentially decrease or increase depending on the energy difference between the intermediate states and initial/final state. Since these unphysical effects are dominated by the ground-state contributions as shown in Fig. 3 and Fig. 4, here we only consider the low-lying states $|n\rangle = |\pi\pi(I = L = 1)\rangle$ for $t > 0$ and $|n_s\rangle = |K\rangle$ for $t < 0$.

For $t > 0$, since we use the gauge ensemble with $m_\pi = 0.3515(15)$ GeV and $m_K = 0.5057(13)$ GeV, $\pi\pi$ states are always heavier than the kaon state. In our numerical study, we do not observe any statistically significant temporal truncation effects and the unphysical contribution from $e^{-(E_{\pi\pi}-E)T/2}$ can be safely neglected.

For $t < 0$, the temporal truncation effects are not negligible especially in the soft photon region, where the electromagnetic current carries vanishing momentum $P = (iE, \vec{p}) \approx (0, \vec{0})$. As a result, the intermediate kaon state has the energy E_K very close to the energy of the initial state m_K . A very large T is required to make the factor $e^{-(E+E_K-m_K)T/2}$ sufficiently small. Unfortunately, this requirement is not satisfied by a typical lattice temporal extent of a few fm. Thus the exponential term $e^{-(E+E_K-m_K)T/2}$ is far from convergence, leading to a large temporal truncation effects.

In our numerical calculation, we find that even beyond the soft photon region, the temporal truncation effects are generally not negligible. It means that we need a systematic improved method to reduce the unphysical contamination from $e^{-(E+E_K-m_K)T/2}$.

2. Finite-volume effects

As explained in Ref. [25], the size of the hadronic function $H^{\mu\nu}(x, Q)$ exponentially suppresses at large spatial separation $|\vec{x}|$. The rate of suppression depends on the energy difference between intermediate state and the initial state. If $H^{\mu\nu}(x, Q)$ does not decrease to zero at the boundary of the lattice, then the finite-volume effects are expected to be non-negligible. In other words, the lattice data $H^{(L),\mu\nu}(x, Q)$ could deviate from the infinite-volume $H^{\mu\nu}(x, Q)$ by a sizeable difference. These finite-volume effects propagate into $H^{\mu\nu}(P, Q)$ and are more enhanced when P is a non-lattice momentum.

In our numerical study, we find that the finite-volume effects for the $t > 0$ integral are negligible. The reasons are two folds. First, the calculation is performed at the unphysical pion mass and the finite-volume effects from $\pi\pi$ states are suppressed. Second, the electromagnetic current significantly couples to a ρ -like state which is much heavier than the kaon state at $m_\pi = 352$ MeV. As a consequence, the finite-volume effects mainly comes from the kaon intermediate state in the $t < 0$ integral.

After the explanation of the origin of both temporal truncation and finite-volume effects, we will start to describe the IVR method to reduce these unphysical systematic effects.

3. Step 1: IVR

In the $t < 0$ region, the hadronic function $H^{\mu\nu}(\vec{x}, t)$ is saturated by the single particle states at sufficiently large $|t|$. We remark such time separation as $|t| > t_s$. For $t \leq -t_s$, the hadronic function can be given by

$$\begin{aligned}
H^{\mu\nu}(\vec{x}, t)|_{t \leq -t_s} &= \langle 0 | J_A^\nu(\vec{0}, 0) J_{\text{em}}^\mu(\vec{x}, t) | K \rangle \\
&= \int \frac{d^3 p_K}{(2\pi)^3 2E_K} \langle 0 | J_A^\nu(\vec{0}, 0) | K(p_K) \rangle \langle K(p_K) | J_{\text{em}}^\mu(\vec{0}, 0) | K \rangle e^{-i\vec{p}_K \cdot \vec{x}} e^{(E_K - m_K)t} \\
&= \int \frac{d^3 p_K}{(2\pi)^3} \tilde{H}^{\mu\nu}(\vec{p}_K, E_K) e^{-i\vec{p}_K \cdot \vec{x}} e^{(E_K - m_K)t}, \tag{34}
\end{aligned}$$

with $\tilde{H}^{\mu\nu}(\vec{p}_K, E_K)$ defined as

$$\tilde{H}^{\mu\nu}(\vec{p}_K, E_K) = \frac{1}{2E_K} \langle 0 | J_A^\nu(\vec{0}, 0) | K(p_K) \rangle \langle K(p_K) | J_{\text{em}}^\mu(\vec{0}, 0) | K \rangle. \quad (35)$$

We can determine $\tilde{H}^{\mu\nu}(\vec{p}_K, E_K)$ using $H^{\mu\nu}(\vec{x}, t)$ at $t = -t_s$ as an input

$$\tilde{H}^{\mu\nu}(\vec{p}_K, E_K) = \int d^3x' H^{\mu\nu}(\vec{x}', -t_s) e^{i\vec{p}_K \cdot \vec{x}'} e^{(E_K - m_K)t_s}. \quad (36)$$

Using the expression of $\tilde{H}^{\mu\nu}(\vec{p}_K, E_K)$ in Eq. (36), all the hadronic function $H^{\mu\nu}(\vec{x}, t)$ with $t < -t_s$ can be reconstructed via

$$\begin{aligned} H^{\mu\nu}(\vec{x}, t) \Big|_{t \leq -t_s} &= \int \frac{d^3p_K}{(2\pi)^3} \tilde{H}^{\mu\nu}(\vec{p}_K, E_K) e^{-i\vec{p}_K \cdot \vec{x}} e^{(E_K - m_K)t} \\ &= \int \frac{d^3p_K}{(2\pi)^3} \int d^3x' H^{\mu\nu}(\vec{x}', -t_s) e^{i\vec{p}_K \cdot (\vec{x}' - \vec{x})} e^{(E_K - m_K)(t + t_s)}. \end{aligned} \quad (37)$$

As a next step, the time integral (28) with the range $-T/2 < t < 0$ can be separated into two parts: $-t_s < t < 0$ and $-T/2 < t < -t_s$. We can extend the lower bound of the integral from $-T/2$ to $-\infty$. By putting Eq. (37) into the integral, we have

$$\begin{aligned} &\int_{-\infty}^0 dt \int d^3\vec{x} e^{Et - i\vec{p} \cdot \vec{x}} H^{\mu\nu}(\vec{x}, t) \\ &= \int_{-t_s}^0 dt \int d^3\vec{x} e^{Et - i\vec{p} \cdot \vec{x}} H^{\mu\nu}(\vec{x}, t) + \int_{-\infty}^{-t_s} dt \int d^3\vec{x} e^{Et - i\vec{p} \cdot \vec{x}} H^{\mu\nu}(\vec{x}, t) \\ &= \int_{-t_s}^0 dt \int d^3\vec{x} e^{Et - i\vec{p} \cdot \vec{x}} H^{\mu\nu}(\vec{x}, t) + \int d^3\vec{x} e^{-i\vec{p} \cdot \vec{x}} H^{\mu\nu}(\vec{x}, -t_s) \frac{e^{-Et_s}}{E + E_K - m_K}. \end{aligned} \quad (38)$$

From the second to the third line, the hadronic function $H^{\mu\nu}(\vec{x}, t)$ with $t < -t_s$ is reconstructed using Eq. (37). Using the hadronic function at some modest value of t_s , it allows us to perform the time integral analytically in the whole region of $-\infty < t < -t_s$. Thus the temporal truncation effects naturally disappear.

In the practical calculation, we use the IVR method to reconstruct the scalar functions $\tilde{I}_i(\rho_1, \rho_2)$. The treatment is very similar as described above. We separate the time integral into the short-distance part with $t > -t_s$ and long-distance part with $t < -t_s$ and obtain $\tilde{I}_i^{(s)}(\rho_1, \rho_2)$ and $\tilde{I}_i^{(l)}(\rho_1, \rho_2)$ correspondingly. The total contribution is a combination of

$$\tilde{I}_i^{\text{IVR}}(\rho_1, \rho_2) = \tilde{I}_i^{(s)}(\rho_1, \rho_2) + \tilde{I}_i^{(l)}(\rho_1, \rho_2), \quad i = 1, \dots, 6. \quad (39)$$

The detailed expressions for $\tilde{I}_i^{(s)}$ and $\tilde{I}_i^{(l)}$ are given in Appendix A.

4. Step 2: δ_{IVR}

After making correction to the temporal truncation effects, the lattice results are still affected by the finite-volume effects, which is denoted as δ_{IVR} here. In Ref. [25], such correction has been demonstrated to be exponentially suppressed as the lattice size L increases. This exponential behavior is also confirmed by our numerical analysis in Sec. IV. We can calculate and correct the leading effect of this already exponentially suppressed finite volume error. Although exponentially suppressed, δ_{IVR} can still be very large if a relatively small lattice (e.g. $La = 2.2$ fm in this calculation) is used.

We evaluate δ_{IVR} as follows. The hadronic function $H^{\mu\nu}(P, Q)$ is calculated using $H^{(L),\mu\nu}(x, Q)$ as an input

$$\begin{aligned}
 H^{\mu\nu}(P, Q) &= \int d^4x e^{Et - i\vec{p}\cdot\vec{x}} H^{\mu\nu}(x, Q) \\
 &= \int_V d^4x e^{Et - i\vec{p}\cdot\vec{x}} H^{(L),\mu\nu}(x, Q) \\
 &\quad + \int_V d^4x e^{Et - i\vec{p}\cdot\vec{x}} (H^{\mu\nu}(x, Q) - H^{(L),\mu\nu}(x, Q)) \\
 &\quad + \int_{>V} d^4x e^{Et - i\vec{p}\cdot\vec{x}} H^{\mu\nu}(x, Q).
 \end{aligned} \tag{40}$$

In the above equation, $\int_V d^4x$ indicates that the integral is carried out within a finite volume, while $\int_{>V} d^4x$ means that the integral is performed outside the lattice box. The second line of Eq. (40) shows the contribution from lattice data $H^{(L),\mu\nu}(x, Q)$. The remaining contributions are given by the third and fourth lines in Eq. (40) and denoted as $\delta_{IVR}^{(1)}$ and $\delta_{IVR}^{(2)}$, respectively. Combining $\delta_{IVR}^{(1)}$ and $\delta_{IVR}^{(2)}$ together yields the so-called correction δ_{IVR} . Our goal is to determine this correction term.

Combining the corrections to the temporal truncation effects and finite-volume effects, the main idea of IVR method can be summarized by Fig. 5.

As the finite-volume effects are dominated by the kaon intermediate state, we can use the kaon contribution to estimate δ_{IVR} . The hadronic function from kaon state in the finite volume can be written as

$$H_K^{(L),\mu\nu}(x, Q) = \frac{1}{L^3} \sum_{\vec{p}} \frac{1}{2E} f_K P^\nu (P + Q)^\mu F^{(K)}(q^2) e^{-i\vec{p}\cdot\vec{x}} e^{(E - m_K)t}, \tag{41}$$

where \vec{p} is summed over discrete momenta in finite volume. $F^{(K)}(q^2)$ is the electromagnetic kaon form factor with $q^2 = -(P - Q)^2$. One can construct $H_K^{(L),\mu\nu}(x, Q)$ in coordinate space

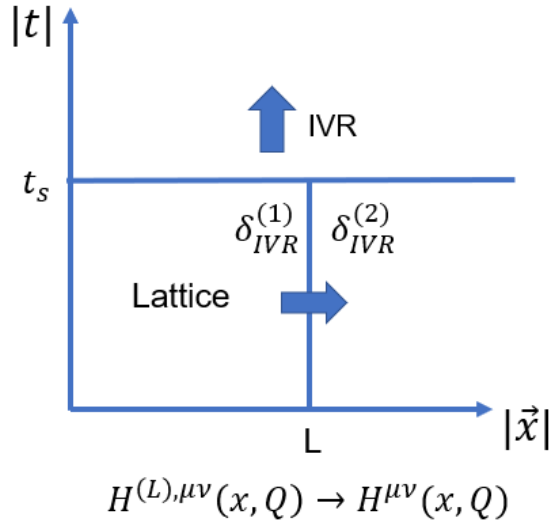


Figure 5. The main idea of IVR method. In the temporal direction, $H^{\mu\nu}(x, Q)|_{t < -t_s}$ is reconstructed by using $H^{\mu\nu}(x, Q)$ at $t = -t_s$. In the spatial direction, the finite-volume effects are corrected by calculating $\delta_{IVR}^{(1)}$ and $\delta_{IVR}^{(2)}$ via the kaon state dominance.

using Fourier transformation if the functional form of $F^{(K)}(q^2)$ is given. When $L \rightarrow \infty$, one can define the infinite-volume kaon contribution via $H_K^{\mu\nu}(x, Q) \equiv \lim_{L \rightarrow \infty} H_K^{(L),\mu\nu}(x, Q)$.

In our numerical analysis, we find that the lattice data of $H^{(L),\mu\nu}(x, Q)$ at $t \leq -12$ can be well described by the function of $H_K^{(L),\mu\nu}(x, Q)$, which is constructed by putting a simple form $F^{(K)}(q^2) = 1 + (r_K^2/6)q^2$ into Eq. (41), with r_K the kaon charge radius. In Fig. 6, we make the plot of the hadronic function $H^{(L),00}(x, Q)$ at $t = -12$ as an example. The consistency between $H^{(L),\mu\nu}(x, Q)$ and $H_K^{(L),\mu\nu}(x, Q)$ has also been checked for other (μ, ν) indices. As shown in Fig. 6, using a rough model with $F^{(K)}(q^2) \equiv 1$, $H_K^{(L),\mu\nu}(x, Q)$ described by the blue curve is already quite close to the lattice data at large $|x|$. The existing deviation suggests that one could determine r_K^2 by fitting the lattice data of $H^{(L),\mu\nu}(x, Q)$ to the form of $H_K^{(L),\mu\nu}(x, Q)$. We use the lattice data with $t \leq -12$ to fit r_K^2 . Although the calculation is performed at the unphysical pion mass, we find that the fitting result $r_K^2 = 0.28(2) \text{ fm}^2$ is consistent with $r_K^2 = 0.31(4) \text{ fm}^2$ from Particle Data Book [36]. By using $r_K^2 = 0.28(2) \text{ fm}^2$ as an input, the result of $H_K^{(L),\mu\nu}(x, Q)$, shown as the green curve in Fig. 6 agrees well with the lattice data of $H^{(L),\mu\nu}(x, Q)$ at long distance.

Based on the agreement between $H^{(L),\mu\nu}(x, Q)$ and $H_K^{(L),\mu\nu}(x, Q)$ at long distance, we use

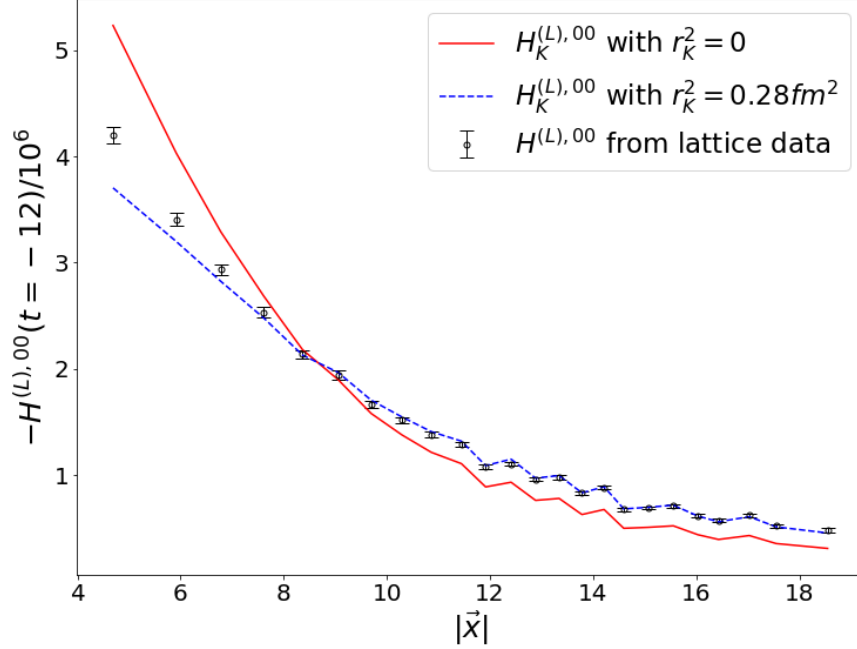


Figure 6. The comparison between lattice data $H_K^{(L),00}(x)$ and kaon theory in finite volume $H_K^{(L),00}(x)$. The red points are lattice result $H_K^{(L),\mu\nu}(x, Q)$. The blue line corresponds to $r_K^2 = 0$, and the green line corresponds to $r_K^2 = 0.28(2) fm^2$.

the kaon-state contribution $H_K^{(L),\mu\nu}(x, Q)$ and $H_K^{\mu\nu}(x, Q)$ to estimate the size of δ_{IVR} through

$$\delta_{\text{IVR}} \approx \int_V d^3\vec{x} e^{Et - i\vec{p}\cdot\vec{x}} (H_K^{\mu\nu}(x, Q) - H_K^{(L),\mu\nu}(x, Q)) + \int_{>V} d^3\vec{x} e^{Et - i\vec{p}\cdot\vec{x}} H_K^{\mu\nu}(x, Q). \quad (42)$$

Using the approach described above, we can also apply the finite-volume correction to the scalar functions and obtain

$$\delta_i^{\text{IVR}}(L) = \tilde{I}_i^{\text{IVR}}(\rho_1, \rho_2) - \tilde{I}_i^{\text{IVR}}(\rho_1, \rho_2; L) \approx \tilde{I}_{i,K}^{\text{IVR}}(\rho_1, \rho_2) - \tilde{I}_{i,K}^{\text{IVR}}(\rho_1, \rho_2; L), \quad (43)$$

where the subscript K is used to indicate the scalar functions compiled from the kaon-intermediate-state contribution. In $\tilde{I}_i^{\text{IVR}}(\rho_1, \rho_2; L)$ and $\tilde{I}_{i,K}^{\text{IVR}}(\rho_1, \rho_2; L)$, a parameter L is introduced to specify the scalar functions in the finite volume. For scalar functions in the infinite volume, $\tilde{I}_{i,K}^{\text{IVR}}(\rho_1, \rho_2)$, it can be approximated by $\tilde{I}_{i,K}^{\text{IVR}}(\rho_1, \rho_2; L_\infty)$ with a sufficiently large L_∞ .

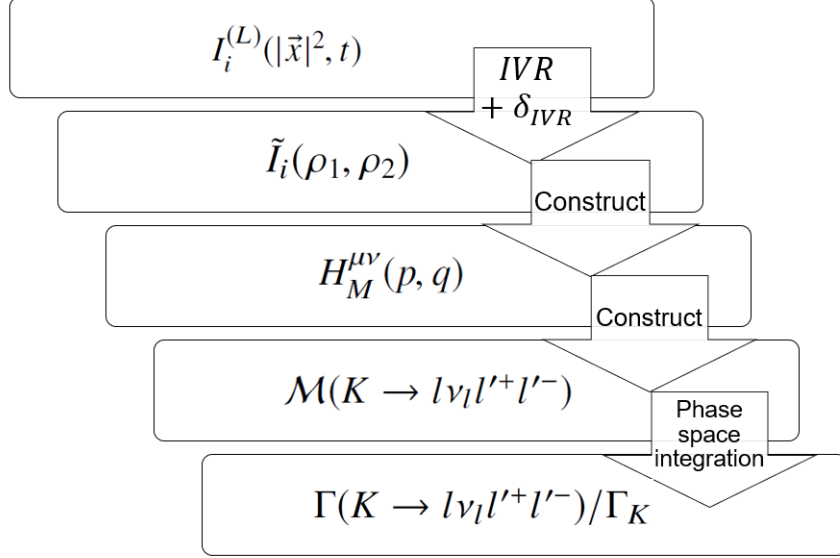


Figure 7. Lattice calculation procedures of the decay width.

D. Computation of the decay width

In this section, we summarize the procedure to compute the decay width of $K \rightarrow \ell\nu\ell'^+\ell'^-$. The outline of the main steps is shown in Fig. 7.

In our calculation, the kaon mass $m_{K,\text{lat}} = 0.5057(13)$ GeV is slightly larger than its physical value $m_{K,\text{phy}} = 0.493677(16)$ GeV [36]. To reduce the influence from the unphysical kaon mass, for all the dimensional quantities $O^{[n]}$ with dimension n , we rescale them as

$$\bar{O}^{[n]} = O^{[n]}\xi_K^n, \quad \xi_K \equiv \frac{m_{K,\text{phy}}}{m_{K,\text{lat}}}. \quad (44)$$

For example, the decay constant and the hadronic function are rescaled as

$$\bar{f}_K = \xi_K f_K, \quad \bar{H}_M^{\mu\nu}(p, q) = \xi_K H_M^{\mu\nu}(p, q). \quad (45)$$

and the decay amplitudes originally defined in Eq. (10) are rescaled as

$$\bar{\mathcal{M}}_D = \xi_K \mathcal{M}_D, \quad \bar{\mathcal{M}}_E = \xi_K \mathcal{M}_E. \quad (46)$$

As the Fermi constant G_F is a fixed coefficient, $\mathcal{M}_{D,E}$ are considered here as the dimension-1 quantities. After the rescaling, we can adopt the physical kaon mass in the phase-space integral to determine the decay width.

For the lattice calculation of $\text{Br}[K \rightarrow \ell\nu_\ell\ell'^+\ell'^-]$ with $\ell = \ell'$, we use the Monte-Carlo integration. Within the allowed phase-space range, the five parameters, $(x_{12}, x_{34}, y_{12}, y_{34}, \phi)$, are

Lable	$L^3 \times T$	a^{-1}	N_{conf}	m_π	m_K	ΔT
cA211b.53.24	$24^3 \times 48$	2.12 GeV	51	0.3515(15) GeV	0.5057(13) GeV	10

Table III. Information of lattice setup.

randomly generated N_{MC} times. Given each momentum setup, $\bar{H}_M^{\mu\nu}(p_{12}, q)$ and $\bar{H}_M^{\mu\nu}(p_{14}, q)$ are calculated using the IVR method. In order to get the decay amplitude in Eq. (46), numerical realization of the spinor products are utilized. The branching ratio is calculated as follows

$$\begin{aligned} \text{Br}[K \rightarrow \ell\nu_\ell\ell^+\ell^-] &= \frac{1}{2m_K\Gamma_K} \int d\Phi_4 \left(|\bar{\mathcal{M}}_D|^2 + |\bar{\mathcal{M}}_E|^2 + 2\text{Re}[\bar{\mathcal{M}}_D\bar{\mathcal{M}}_E^*] \right) \\ &= \frac{1}{2m_K\Gamma_K} \frac{S}{N_{MC}} \sum_{i=1}^{N_{MC}} \frac{\mathcal{S}\lambda m_K^4}{2^{14}\pi^6} \left(|\bar{\mathcal{M}}_D|^2 + |\bar{\mathcal{M}}_E|^2 + 2\text{Re}[\bar{\mathcal{M}}_D\bar{\mathcal{M}}_E^*] \right)_i \end{aligned} \quad (47)$$

where S is the hypervolume of the integration range and $m_K = m_{K,\text{phy}}$.

In the practical calculation, we choose $N_{MC} = 10000$, and confirm that the Monte-Carlo error is much less than the statistical error. Considering the fact that the construction of the scalar functions is nontrivial, the Monte-Carlo integration thus provides an easily implemented approach to determine the decay width.

IV. NUMERICAL RESULTS

A. Lattice setup

In the lattice calculation, we use a gauge ensemble with $N_f = 2 + 1 + 1$ -flavor twisted mass fermion generated by ETM Collaboration [37]. The light quark mass is unphysical with $m_\pi = 352$ MeV. We tune the valence strange quark mass to have the kaon mass close to its physical value. Parameters of the gauge ensemble are listed in Tabel III together with the information of ΔT , whose value shall be set sufficiently large to suppress the excited-state contamination.

In order to calculate hadronic functions, three-point correlation functions are calculated on lattice. The initial kaon state is created using Coulomb gauge-fixed wall source operator. We place two point-source propagators and one wall-source propagator at each time slice and perform a time translation average over all time slices to the three-point function.

B. Results

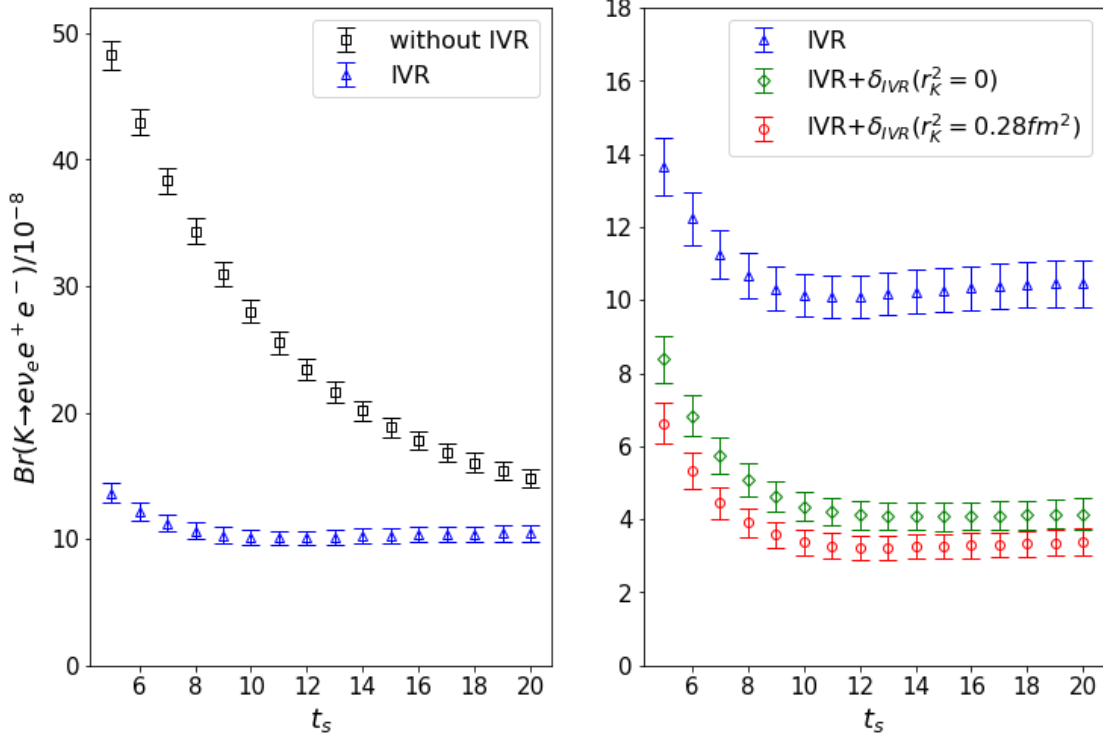


Figure 8. IVR results for $K \rightarrow \nu_e e^+ e^-$ ($L_\infty = 72$). In the left-hand panel, a comparison is made between the results with and without IVR correction. In the right-hand panel, a comparison is made among the results with various δ_{IVR} corrections.

In Fig. 8, we take $K \rightarrow \nu_e e^+ e^-$ as an example to show the results of branching ratio using IVR method with different t_s . In the left-hand panel, a comparison is made between the results with and without an IVR correction. A significant temporal truncation effect is found, demonstrating the importance of the IVR correction. The time t_s needs to be sufficiently large to guarantee the ground-intermediate-state dominance. The figure shows that starting from $t_s \approx 12$, the branching ratio is independent from the choice of t_s .

In the right-hand panel of Fig. 8, the effects of δ_{IVR} are shown. Here the δ_{IVR} correction is made with the choice of $L_\infty = 72$. We find that it is essential to include the correction δ_{IVR} . Comparison between the results with $r_K^2 = 0$ (green data) and $r_K^2 = 0.28(2) \text{ fm}^2$ (red data) indicates that the correction from the r_K^2 -term is non-negligible but its size is still quite small (about two times of the statistical error). We also tried with higher-order corrections and found that the effects are negligible. We thus quote with result with $r_K^2 = 0.28(2) \text{ fm}^2$

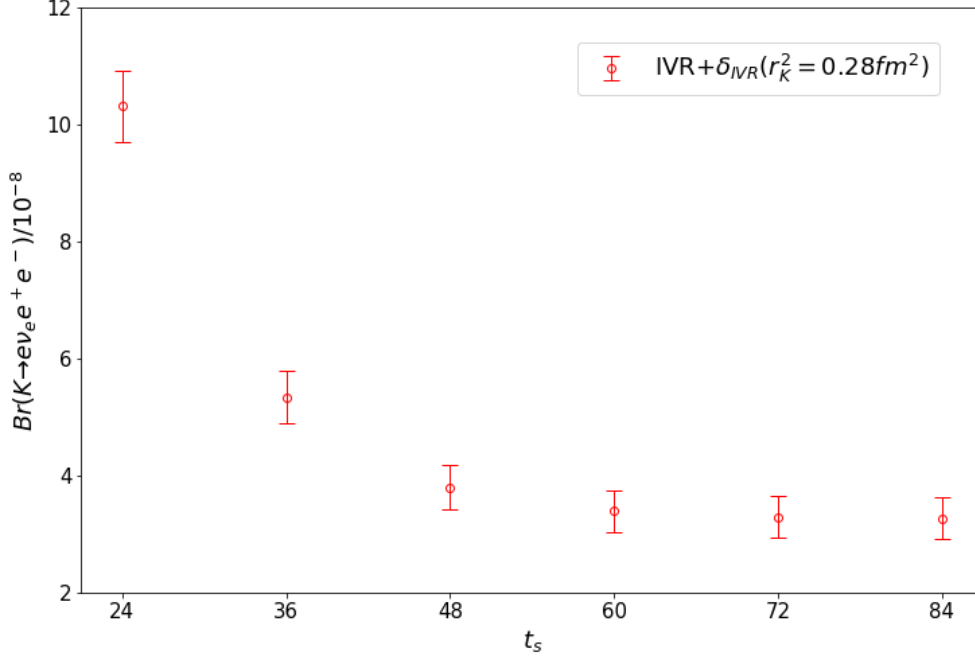


Figure 9. Examination of L_∞ -dependence in the δ_{IVR} correction using $K \rightarrow e \nu_e e^+ e^-$ decay as an example. The lattice with a spatial extent L_∞ is used to approximate the infinite-volume lattice. When $L_\infty = L = 24$, no correction is made and $\delta_{IVR} = 0$. By increasing L_∞ , δ_{IVR} exponentially converges and $L_\infty = 72$ is a sufficiently large lattice size to approximate the infinite one.

as the final results.

For the results shown in Fig. 8, the parameter L_∞ is chosen as $L_\infty = 72$. In Fig. 9 we examine the L_∞ -dependence of the results. We confirm that as L_∞ increases, the finite-volume effects exponentially suppress and $L_\infty = 72$ is an appropriate choice to approximate the infinitely large spatial extent.

In Fig. 10, IVR results for all the four channels of $K \rightarrow \ell \nu_\ell \ell'^+ \ell'^-$ are shown. The final results of branching ratio are already shown in Table I. These results are compiled using $r_K^2 = 0.28(2) \text{ fm}^2$, fitting range $t_s \in [12, 17]$ and $L_\infty = 72$. We find that the lattice results are close to experimental or ChPT ones. The systematic errors of our results mainly come from unphysical quark masses and lattice artifacts, which leaves for a future study.

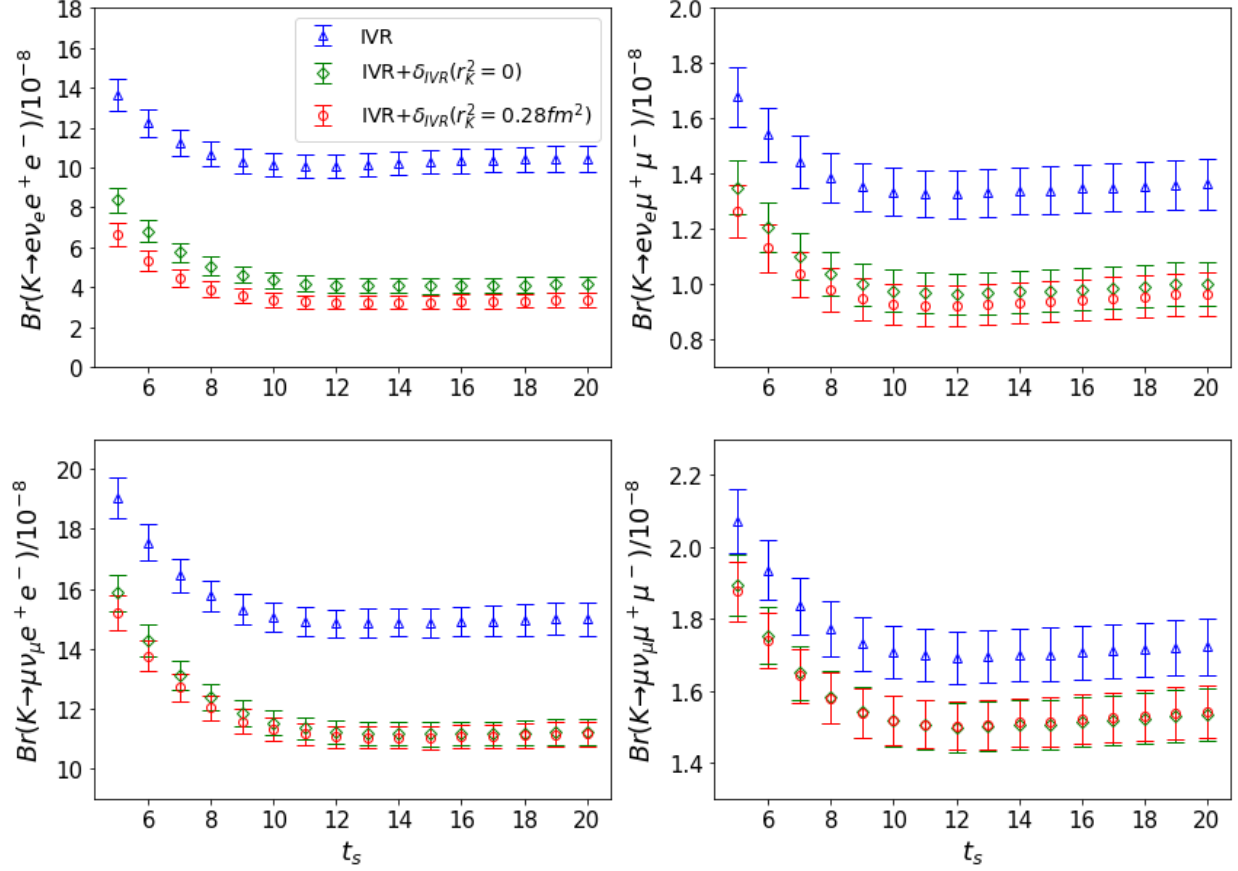


Figure 10. IVR results for four channels of $K \rightarrow l\nu_\ell\ell'^+\ell'^-$. The upper-left figure for $K \rightarrow e\nu_e e^+e^-$ has been shown in the right-hand panel of Fig. 8. We put it here for the sake of an easier comparison with other three channels. Through the comparison we find that the δ_{IVR} corrections are important for all the channels. But the contributions from the r_K^2 terms are less significant for the other three channels.

V. CONCLUSION

In this work, we build a lattice calculation procedure to determine $K \rightarrow l\nu_\ell\ell'^+\ell'^-$ decay width by solving a series of technical problems. IVR method is used to reduce temporal truncation effects and finite-volume effects. Other approaches, such as scalar function method and Monte-Carlo phase-space integration, are proposed to simplify the calculation. Using these techniques, a practical methodology is developed to compute decay width with four daughter particles in the final state, as summarized in Fig. 7.

Using this methodology, we perform a realistic lattice calculation of $K \rightarrow l\nu_\ell\ell'^+\ell'^-$ decay

width using an ensemble with pion mass 352 MeV and kaon mass 506 MeV, and obtain the branching ratios close to ChPT or experimental results. Through the calculation, we demonstrate the capability of lattice QCD to improve Standard Model prediction in $K \rightarrow \ell\nu_\ell\ell'^+\ell'^-$ decay width. By examining the t_s -dependence and L_∞ -dependence of decay width, we show that the IVR method is a vital approach to reduce the systematic effects. Future work is still required to address the power-law finite-volume effects in the subprocess of $K \rightarrow \pi\pi\ell\nu_\ell \rightarrow \ell\nu_\ell\ell'^+\ell'^-$ and make a full control of various systematic effects.

ACKNOWLEDGMENTS

We thank Guido Martinelli for giving an inspiring lecture at the lattice QCD summer school held at Peking University on 2019, which motivates this work. We thank ETM Collaboration for sharing the gauge configurations with us. X.F. and L.C.J. gratefully acknowledge many helpful discussions with our colleagues from the RBC-UKQCD Collaboration. X.F., X.Y.T. and T.W. are supported in part by NSFC of China under Grant No. 11775002 and No. 12070131001 and National Key Research and Development Program of China under Contracts No. 2020YFA0406400. L.C.J. acknowledges support by DOE Office of Science Early Career Award DE-SC0021147 and DOE grant DE-SC0010339. The calculation was carried out on TianHe-3 (prototype) at Chinese National Supercomputer Center in Tianjin.

Appendix A: Formulae in scalar function method

1. Infinite-volume case

In Sec. III, the scalar function method is described by Eqs. (30) and (33). In this section, we will give the detailed expression to calculate $\tilde{I}_i(\rho_1, \rho_2)$ and then discuss the approach to construct $H^{\mu\nu}(P, Q)$ using the scalar functions.

We start with the relation

$$H^{\mu\nu}(P, Q) = -i \int d^4x e^{Et - i\vec{p}\cdot\vec{x}} H^{\mu\nu}(x, Q). \quad (\text{A1})$$

Combining Eq. (A1) with the Lorentz factors given in Eq. (29), we can obtain the relation

between $\tilde{I}_i(\rho_1, \rho_2)$ and $I_i(|\vec{x}|^2, t)$. Here we give the detailed expressions of $\tilde{I}_i(\rho_1, \rho_2)$ as

$$\tilde{I}_1(\rho_1, \rho_2) = -m_K^2 \int d^4x e^{Et} j_0(\varphi) I_1(|\vec{x}|^2, t), \quad (\text{A2a})$$

$$\tilde{I}_2(\rho_1, \rho_2) = -m_K^2 \int d^4x e^{Et} j_0(\varphi) I_2(|\vec{x}|^2, t), \quad (\text{A2b})$$

$$\tilde{I}_3(\rho_1, \rho_2) = -m_K E \int d^4x e^{Et} j_0(\varphi) I_2(|\vec{x}|^2, t) + m_K |\vec{p}| \int d^4x e^{Et} \frac{j_1(\varphi)}{|\vec{x}|} I_3(|\vec{x}|^2, t), \quad (\text{A2c})$$

$$\tilde{I}_4(\rho_1, \rho_2) = -m_K E \int d^4x e^{Et} j_0(\varphi) I_2(|\vec{x}|^2, t) + m_K |\vec{p}| \int d^4x e^{Et} \frac{j_1(\varphi)}{|\vec{x}|} I_4(|\vec{x}|^2, t), \quad (\text{A2d})$$

$$\begin{aligned} \tilde{I}_5(\rho_1, \rho_2) = & -E^2 \int d^4x e^{Et} j_0(\varphi) I_2(|\vec{x}|^2, t) - |\vec{p}|^2 \int d^4x e^{Et} \frac{j_2(\varphi)}{|\vec{x}|^2} I_5(|\vec{x}|^2, t) \\ & + |\vec{p}| \int d^4x e^{Et} \frac{j_1(\varphi)}{|\vec{x}|} [EI_3(|\vec{x}|^2, t) + EI_4(|\vec{x}|^2, t) + I_1(|\vec{x}|^2, t) - I_2(|\vec{x}|^2, t)] \end{aligned} \quad (\text{A2e})$$

$$\tilde{I}_6(\rho_1, \rho_2) = m_K |\vec{p}| \int d^4x e^{Et} \frac{j_1(\varphi)}{|\vec{x}|} I_6(|\vec{x}|^2, t). \quad (\text{A2f})$$

Note that in the continuum theory, the scalar functions $\tilde{I}_i(\rho_1, \rho_2)$ do not depend on the direction of \vec{p} . Thus, in the derivation of the above equations we have performed an average over the solid angle of \vec{p} . After the average, the factor $e^{-i\vec{p}\cdot\vec{x}}$ is converted into a spherical Bessel function $j_0(\varphi)$, with $\varphi = |\vec{p}||\vec{x}|$. In total, three spherical Bessel functions appear in Eq. (A2). They take the standard definition as

$$j_0(\varphi) \equiv \frac{\sin \varphi}{\varphi}, \quad j_1(\varphi) \equiv \frac{\sin \varphi - \varphi \cos \varphi}{\varphi^2}, \quad j_2(\varphi) \equiv \frac{(3 - \varphi^2) \sin \varphi - 3\varphi \cos \varphi}{\varphi^3}. \quad (\text{A3})$$

In the numerical calculation, when the variables ρ_1 and ρ_2 are given, the values of $|\vec{p}|$ and E can be determined through

$$|\vec{p}| = \frac{1}{2} m_K \sqrt{(1 + \rho_1 - \rho_2)^2 - 4\rho_1}, \quad E = \frac{1}{2} m_K (1 + \rho_1 - \rho_2). \quad (\text{A4})$$

Once these scalar functions $\tilde{I}_i(\rho_1, \rho_2)$ are available, $H^{\mu\nu}(P, Q)$ can be easily constructed using Eq. (30). In numerical calculation, $w_i(P, Q)$ in Eq. (30) is implicitly derived using following procedures:

1. A general factorization of $H^{\mu\nu}(P, Q)$ is used with

$$\begin{aligned} H^{\mu\nu}(P, Q) = & a(\rho_1, \rho_2) P^\mu Q^\nu + b(\rho_1, \rho_2) P^\nu Q^\mu + c(\rho_1, \rho_2) P^\mu P^\nu \\ & + d(\rho_1, \rho_2) Q^\mu Q^\nu + e(\rho_1, \rho_2) \delta^{\mu\nu} m_K^2 + f(\rho_1, \rho_2) \epsilon^{\mu\nu\alpha\beta} P^\alpha Q^\beta. \end{aligned} \quad (\text{A5})$$

2. $\tilde{I}_i(\rho_1, \rho_2)$ ($i = 1 \dots 6$) and $a(\rho_1, \rho_2), \dots, f(\rho_1, \rho_2)$ are related by a simple linear transformation. We can then solve the solution for $a(\rho_1, \rho_2), \dots, f(\rho_1, \rho_2)$ and construct $H^{\mu\nu}(P, Q)$ using Eq. (A5).

It should be kept in mind that, in the continuum theory $\tilde{I}_i(\rho_1, \rho_2)$ for $i = 1, \dots, 6$ are not fully independent due to the constraint from Ward identity (4). However, in the lattice calculation, Ward identity is violated due to the lattice artifacts and finite-volume effects. Thus we discard the constraint from Ward identity. It allows us to use six scalar functions with very simple form, as shown in Eqs. (29) and (32).

2. Scalar functions with the IVR corrections

In Sec. III, IVR method is proposed to correct the temporal truncation effects and the finite volume effects for the hadronic functions $H^{\mu\nu}(P, Q)$. In this section, we show how to apply the IVR method to the scalar functions.

We shall point out first that the calculation of $\tilde{I}_6(\rho_1, \rho_2)$ does not require the IVR correction. It is because $\tilde{I}_6(\rho_1, \rho_2)$ is projected out by using the Lorentz factor of $\epsilon_{\mu\nu\alpha\beta}P^\alpha Q^\beta$. In this quantity, the intermediate states are given by the states heavier than initial kaon state and thus the temporal truncation effects and finite-volume effects can be neglected.

In the calculation of $\tilde{I}_i(\rho_1, \rho_2)$, with $i = 1, \dots, 5$, we also use $t = -t_s$ to separate the time integral into the short-distance part and the long-distance part

$$\tilde{I}_i(\rho_1, \rho_2) = \tilde{I}_i^{(s)}(\rho_1, \rho_2) + \tilde{I}_i^{(l)}(\rho_1, \rho_2). \quad (\text{A6})$$

For the short-distance part, we replace $\tilde{I}_i^{(s)}(\rho_1, \rho_2)$ by the lattice data $\tilde{I}_i^{(s)}(\rho_1, \rho_2, L)$. For the long-distance part, we use the lattice data of $I_i^{(L)}(|\vec{x}|^2, t)$ at $t = -t_s$ as input. Through the kaon-intermediate-state dominance, $\tilde{I}_i^{(l)}(\rho_1, \rho_2, L)$ can be reconstructed. The detailed expressions are given as

$$\tilde{I}_1^{(l)}(\rho_1, \rho_2; L) = -\frac{m_K^2}{E + E_K - m_K} \int d^3\vec{x} e^{-Et_s} j_0(\varphi) I_1^{(L)}(|\vec{x}|^2, t_s), \quad (\text{A7a})$$

$$\tilde{I}_2^{(l)}(\rho_1, \rho_2; L) = -\frac{m_K^2}{E + E_K - m_K} \int d^3\vec{x} e^{-Et_s} j_0(\varphi) I_2^{(L)}(|\vec{x}|^2, t_s), \quad (\text{A7b})$$

$$\begin{aligned} \tilde{I}_3^{(l)}(\rho_1, \rho_2; L) = & -\frac{m_K}{E + E_K - m_K} \left[E \int d^3\vec{x} e^{-Et_s} j_0(\varphi) I_2^{(L)}(|\vec{x}|^2, t_s) \right. \\ & \left. + |\vec{p}| \int d^3\vec{x} e^{-Et_s} \frac{j_1(\varphi)}{|\vec{x}|} I_3^{(L)}(|\vec{x}|^2, t_s) \right], \end{aligned} \quad (\text{A7c})$$

$$\begin{aligned} \tilde{I}_4^{(l)}(\rho_1, \rho_2; L) = & -\frac{m_K}{E + E_K - m_K} \left[E \int d^3\vec{x} e^{-Et_s} j_0(\varphi) I_2^{(L)}(|\vec{x}|^2, t_s) \right. \\ & \left. + |\vec{p}| \int d^3\vec{x} e^{-Et_s} \frac{j_1(\varphi)}{|\vec{x}|} I_4^{(L)}(|\vec{x}|^2, t_s) \right], \end{aligned} \quad (\text{A7d})$$

$$\begin{aligned} \tilde{I}_5^{(l)}(\rho_1, \rho_2; L) = & -\frac{m_K}{M(E + E_K - m_K)} \left[E^2 \int d^3\vec{x} e^{-Et_s} j_0(\varphi) I_2^{(L)}(|\vec{x}|^2, t_s) \right. \\ & \left. + |\vec{p}| \int d^3\vec{x} e^{-Et_s} \frac{j_1(\varphi)}{|\vec{x}|} \right. \\ & \times [E I_3^{(L)}(|\vec{x}|^2, t_s) + E I_4^{(L)}(|\vec{x}|^2, t_s) + I_1^{(L)}(|\vec{x}|^2, t_s) - I_2^{(L)}(|\vec{x}|^2, t_s)] \\ & \left. - |\vec{p}|^2 \int d^3\vec{x} e^{-Et_s} \frac{j_2(\varphi)}{|\vec{x}|^2} I_5^{(L)}(|\vec{x}|^2, t_s) \right]. \end{aligned} \quad (\text{A7e})$$

The scalar functions calculated through the IVR method are given by

$$\tilde{I}_i^{\text{IVR}}(\rho_1, \rho_2; L) = \tilde{I}_i^{(s)}(\rho_1, \rho_2; L) + \tilde{I}_i^{(l)}(\rho_1, \rho_2; L), \quad \text{for } i = 1, \dots, 5. \quad (\text{A8})$$

As a next step, we perform the finite-volume correction by introducing $\delta_i^{\text{IVR}}(L)$ for each scalar function

$$\tilde{I}_i(\rho_1, \rho_2) = \tilde{I}_i^{\text{IVR}}(\rho_1, \rho_2; L) + \delta_i^{\text{IVR}}(L). \quad (\text{A9})$$

Here $\delta_i^{\text{IVR}}(L)$ can be approximated by the kaon state contribution

$$\delta_i^{\text{IVR}}(L) \approx \tilde{I}_{i,K}^{\text{IVR}}(\rho_1, \rho_2) - \tilde{I}_{i,K}^{\text{IVR}}(\rho_1, \rho_2; L). \quad (\text{A10})$$

In practice, $\tilde{I}_{i,K}^{\text{IVR}}(\rho_1, \rho_2)$ in the infinite volume can be replaced by $\tilde{I}_{i,K}^{\text{IVR}}(\rho_1, \rho_2; L_\infty)$ with $L_\infty \gg L$.

[1] V. Cirigliano, G. Ecker, H. Neufeld, A. Pich, and J. Portoles, Rev. Mod. Phys. **84**, 399 (2012), arXiv:1107.6001 [hep-ph].

- [2] A. J. Buras, *Acta Phys. Polon. B* **49**, 1043 (2018), arXiv:1805.11096 [hep-ph].
- [3] A. A. Poblaguev *et al.*, *Phys. Rev. Lett.* **89**, 061803 (2002), arXiv:hep-ex/0204006 [hep-ex].
- [4] H. Ma *et al.*, *Phys. Rev. D* **73**, 037101 (2006), arXiv:hep-ex/0505011.
- [5] J. Bijnens, G. Ecker, and J. Gasser, *Nucl. Phys. B* **396**, 81 (1993), arXiv:hep-ph/9209261.
- [6] C. Geng, I.-L. Ho, and T. Wu, *Nucl. Phys. B* **684**, 281 (2004), arXiv:hep-ph/0306165.
- [7] L. Ametller, J. Bijnens, A. Bramon, and F. Cornet, *Phys. Lett. B* **303**, 140 (1993), arXiv:hep-ph/9302219.
- [8] N. H. Christ, X. Feng, A. Portelli, and C. T. Sachrajda (RBC, UKQCD), *Phys. Rev.* **D93**, 114517 (2016), arXiv:1605.04442 [hep-lat].
- [9] Z. Bai, N. H. Christ, X. Feng, A. Lawson, A. Portelli, and C. T. Sachrajda, *Phys. Rev. Lett.* **118**, 252001 (2017), arXiv:1701.02858 [hep-lat].
- [10] Z. Bai, N. H. Christ, X. Feng, A. Lawson, A. Portelli, and C. T. Sachrajda, *Phys. Rev. D* **98**, 074509 (2018), arXiv:1806.11520 [hep-lat].
- [11] N. H. Christ, X. Feng, A. Portelli, and C. T. Sachrajda (RBC, UKQCD), *Phys. Rev. D* **100**, 114506 (2019), arXiv:1910.10644 [hep-lat].
- [12] N. H. Christ, X. Feng, A. Portelli, and C. T. Sachrajda (RBC, UKQCD), *Phys. Rev.* **D92**, 094512 (2015), arXiv:1507.03094 [hep-lat].
- [13] N. H. Christ, X. Feng, A. Juttner, A. Lawson, A. Portelli, and C. T. Sachrajda, *Phys. Rev.* **D94**, 114516 (2016), arXiv:1608.07585 [hep-lat].
- [14] N. Carrasco, V. Lubicz, G. Martinelli, C. T. Sachrajda, N. Tantalo, C. Tarantino, and M. Testa, *Phys. Rev.* **D91**, 074506 (2015), arXiv:1502.00257 [hep-lat].
- [15] V. Lubicz, G. Martinelli, C. T. Sachrajda, F. Sanfilippo, S. Simula, and N. Tantalo, *Phys. Rev.* **D95**, 034504 (2017), arXiv:1611.08497 [hep-lat].
- [16] D. Giusti, V. Lubicz, G. Martinelli, C. T. Sachrajda, F. Sanfilippo, S. Simula, N. Tantalo, and C. Tarantino, *Phys. Rev. Lett.* **120**, 072001 (2018), arXiv:1711.06537 [hep-lat].
- [17] X. Feng, M. Gorchtein, L.-C. Jin, P.-X. Ma, and C.-Y. Seng, *Phys. Rev. Lett.* **124**, 192002 (2020), arXiv:2003.09798 [hep-lat].
- [18] N. H. Christ, X. Feng, L.-C. Jin, and C. T. Sachrajda, *PoS LATTICE2019*, 259 (2020).
- [19] A. Desiderio *et al.*, *Phys. Rev. D* **103**, 014502 (2021), arXiv:2006.05358 [hep-lat].
- [20] R. Frezzotti, M. Garofalo, V. Lubicz, G. Martinelli, C. T. Sachrajda, F. Sanfilippo, S. Simula, and N. Tantalo, (2020), arXiv:2012.02120 [hep-ph].

- [21] P.-X. Ma, X. Feng, M. Gorchtein, L.-C. Jin, and C.-Y. Seng, (2021), arXiv:2102.12048 [hep-lat].
- [22] N. H. Christ, X. Feng, G. Martinelli, and C. T. Sachrajda, Phys. Rev. D **91**, 114510 (2015), arXiv:1504.01170 [hep-lat].
- [23] R. A. Briceño, Z. Davoudi, M. T. Hansen, M. R. Schindler, and A. Baroni, Phys. Rev. D **101**, 014509 (2020), arXiv:1911.04036 [hep-lat].
- [24] N. H. Christ, X. Feng, L. Jin, C. Tu, and Y. Zhao, PoS **LATTICE2019**, 128 (2020).
- [25] X. Feng and L. Jin, Phys. Rev. D **100**, 094509 (2019), arXiv:1812.09817 [hep-lat].
- [26] K. Kampf, J. r. Novotn?, and P. Sanchez-Puertas, Phys. Rev. D **97**, 056010 (2018), arXiv:1801.06067 [hep-ph].
- [27] P. A. Zyla *et al.* (Particle Data Group), PTEP **2020**, 083C01 (2020).
- [28] L. Lellouch and M. Luscher, Commun. Math. Phys. **219**, 31 (2001), arXiv:hep-lat/0003023.
- [29] H. B. Meyer, Phys. Rev. Lett. **107**, 072002 (2011), arXiv:1105.1892 [hep-lat].
- [30] X. Feng, S. Aoki, S. Hashimoto, and T. Kaneko, Phys. Rev. D **91**, 054504 (2015), arXiv:1412.6319 [hep-lat].
- [31] C. Andersen, J. Bulava, B. Hörz, and C. Morningstar, Nucl. Phys. B **939**, 145 (2019), arXiv:1808.05007 [hep-lat].
- [32] F. Erben, J. R. Green, D. Mohler, and H. Wittig, Phys. Rev. D **101**, 054504 (2020), arXiv:1910.01083 [hep-lat].
- [33] X.-Y. Tuo, X. Feng, and L.-C. Jin, Phys. Rev. D **100**, 094511 (2019), arXiv:1909.13525 [hep-lat].
- [34] X. Feng, Y. Fu, and L.-C. Jin, Phys. Rev. D **101**, 051502 (2020), arXiv:1911.04064 [hep-lat].
- [35] N. H. Christ, X. Feng, L.-C. Jin, and C. T. Sachrajda, (2020), arXiv:2009.08287 [hep-lat].
- [36] M. Tanabashi *et al.* (Particle Data Group), Phys. Rev. D **98**, 030001 (2018).
- [37] C. Alexandrou *et al.*, Phys. Rev. D **98**, 054518 (2018), arXiv:1807.00495 [hep-lat].